Seventh International Symp. on Magnetic Bearings, August 23-25 , 2000, ETH Zurich **589**

ELECTROMAGNETIC FORCES CAUSED BY CAGE INDUCTION MOTOR

Erkki Lantto
High Speed Tech Oy, Espoo, Finland, erkki.lantto@highspeedtech.fi

Antero Arkkio, Matti Antila, Kalle Pokki, Andras Simon
Helsinki University of Technology, Laboratory of Electromechanics; Espoo, Finland
antero.arkkio@hut.fi, matti.antila@akumiitti.fi, kpokki@cc.hut.fi, simona1@eng.auburn.edu

ABSTRACT
The paper deals with the forces acting between the rotor and stator of a cage induction motor when the rotor is performing cylindrical whirling motion. Time-stepping finite element analysis is used for solving the magnetic field, and the forces are calculated from the air-gap field based on the principle of virtual work. The forces are measured with a test motor equipped with active magnetic bearings. A simple analytic model is given for rotor dynamic analysis purposes. This model accurately predicts the behaviour of the low frequency force component also in transient situations. Finally, the effects of the magnetic forces on rotor dynamics are briefly discussed.

INTRODUCTION
In magnetic bearing applications, the electric motor is often large compared with the bearings, and the flux densities in the motor and bearings are of about the same magnitude. Therefore, the electric motor may produce significant disturbance forces and change the system dynamics. In this paper we study, what kind of forces there exists, how they can be modelled and taken into consideration in the rotor dynamic analysis.

This paper focuses on the forces acting on a rotor performing cylindrical circular whirling motion with respect to the stator. In this motion, the geometric centrelines of the rotor and stator are aligned but the former moves around the later in a circular orbit with a frequency, called whirling frequency and with a radius, called whirling radius. The forces are studied as functions of the whirling frequency and whirling radius. To simplify the task, we concentrate on the first harmonic force component, i.e. the force at whirling frequency.

A whirling, eccentric rotor creates a non-symmetric flux distribution that causes the forces. The non-ideal field induces circulating currents in the rotor cage and parallel branches of the stator winding. These currents tend to equalise the flux distribution, and by doing this, they may significantly reduce the radial force in the direction of the shortest air gap but, simultaneously, they produce a tangential force.

Conventionally, the forces acting between the rotor and stator have been calculated by analytic means. The most complete analytic model for a whirling rotor in induction machines was developed by Früchtenicht et al. [1]. Their model takes into account the equalising currents induced in the rotor cage but neglects the magnetic saturation of iron and the high-frequency forces associated with the stator and rotor slotting. They also considered the equations of motion of the rotor, and showed that the tangential forces have a significant effect on the stability of the motion.

Numerical field computation methods for analysing the effects of eccentric rotors have been available for about ten years. Arkkio&Lindgren [2] studied the forces in a high-speed motor using time-stepping finite-element analysis. They considered static eccentricity, and the method of analysis was verified by comparing the measured and computed forces. Some more references to analytic methods can be found from this paper.

2 METHODS OF ANALYSIS

2.1 Numerical computation
The magnetic field in the core region and air gap of the motor is assumed to be two-dimensional. It is solved using time-stepping, finite-element analysis. The details of the method have been presented in References [3] and [2].

The electromagnetic force was computed using the method presented by Coulomb [4]. The method is based on the principle of virtual work, and the force is integrated from the air-gap field. This method was chosen as it and other methods based on a similar

integration have given good results when computing the torque of electric machines [3], [5] and the radial force in active magnetic bearings [6].
The whirling motion was produced by changing the finite-element mesh in the air gap. The centre point of the rotor was moved along a circular path at constant speed. In addition, the rotor was rotated at the mechanical angular frequency. Second-order, triangular elements were used. A typical finite element mesh for the cross section of the motor contained about 10 000 nodes.

2.2 Basic results from an analytic model

Früchtenicht et al. [1] developed an analytic model for the circular whirling motion in which they took into account the effects of the equalising currents in the rotor cage. Their basic results are briefly summarised below.
The analytic models of induction machines are usually based on the Fourier decomposition of the magnetic field in the air-gap of the machine. The flux density is presented as a sum of harmonic flux-density waves moving in the air gap either in the positive or negative direction. An eccentric rotor produces two additional harmonics in the air gap field. These eccentricity harmonics are of the form

$$b_{p\pm1}(x,t) = B_{p\pm1}\cos\left[(p\pm1)x - (\omega_1 \pm \omega_w)t - (\varphi_p \pm \varphi_w)\right], \quad (1)$$

where p is the number of pole pairs of the machine, ω_1 is the fundamental frequency, ω_w is the whirling frequency and φ_p and φ_w are phase angles. The eccentricity harmonics interact with the fundamental harmonic of the machine and generate the largest forces. The speed of a circulating harmonic wave often differs from the speed of the rotor. The slips of the rotor with respect to the two eccentricity harmonics are

$$s_{p\pm1} = 1 - \frac{p\pm1}{p}\frac{\omega_1}{\omega_1 \pm \omega_w}(1-s), \quad (2)$$

where s is the slip of the rotor with respect to the fundamental harmonic. If the slip of an eccentricity harmonic is non-zero, the harmonic induces eddy currents in the rotor cage. The eddy currents modify the amplitude and phase of the eccentricity harmonic, and by doing this they affect the radial force. In general, the force component in the direction of the shortest air gap (radial component) is reduced, and a new force component perpendicular to the direction of the shortest air gap (tangential component) is generated.
The slips of the two eccentricity harmonics become zero at whirling frequencies

$$\omega_w = \frac{1 - s(1\pm p)}{p}\omega_1. \quad (3)$$

2.3 Low-order model

The finite element analysis is time consuming, and a lower order model is needed for rotor dynamic studies. The model presented by Früchtenicht et al. [1] becomes compact when a complex rotor dynamic formulation is used

$$\begin{aligned} p_C(t) &= p_X(t) + ip_Y(t), \\ F_C(t) &= F_X(t) + iF_Y(t), \end{aligned} \quad (4)$$

where p is rotor displacement, F is force caused by motor and subscripts X and Y refer to X and Y directions, respectively. Using this formulation, we can write the analytic model [1] as

$$F_C(t) = K(s)p_C e^{i\omega t}, \quad (5)$$

where $s = i\omega$ and p_C is a constant complex number. The frequency response function K can be parameterised as

$$K(s) = k_0 + \frac{k_{p-1}}{s - z_{p-1}} + \frac{k_{p+1}}{s - z_{p+1}}. \quad (6)$$

The k parameters are real valued variables proportional to the square of the fundamental flux density in the air gap. The imaginary parts of the poles z are the whirling frequencies at which the slips of the two eccentricity harmonics become zero (Eq. 3). The real parts of the poles z depend on the dimensions of the machine but not on flux or loading.
The analytic model was developed for circular whirling motion. However, the physical background and the linear spatial behaviour suggest that Eq. (6) can be interpreted as a transfer function model

$$F_C(s) = K(s)p_C(s), \quad (7)$$

where s is the Laplace variable. This transfer function model and the corresponding differential equations can be used to predict the transient response and rotor-dynamic stability as well. This was verified by computing transient responses using FEM simulations and according to Eq. (7). Such a comparison is shown in Figure 6. The results match very well.
When using Eq. (6), we estimate the parameters from the results of the time-stepping, finite element analysis. In this way, we include the effects of core saturation in the model. The imaginary parts of the poles are forced to be equal to the whirling frequencies at which the slips of the two eccentricity harmonics are zero (Eq. 3). In the parameter fitting, we used real k values, according to the analytic theory. A complex fit gives a little better match, especially, at whirling frequencies close to the synchronous frequency. We assume that the imaginary parts of k coefficients are associated with the coupling between the eccentricity harmonics caused by core

saturation. However, from the point of view of rotor dynamics, the fitting of real values gives sufficiently accurate results.

3 METHOD OF MEASUREMENT

The test machine is a 15 kW four-pole cage induction motor. Its main parameters are given in Table 1. The motor was equipped with magnetic bearings to measure the forces. Only radial bearings were installed. The electrical motor acts as an axial bearing. The radial bearings were ordinary 8-pole hetero polar bearings with bias current linearisation. Magnetic bearing operation and the parameters of this particular bearing type are listed by Lantto [7].

TABLE 1: Parameters of the test motor.

Parameter	
Number of poles	4
Number of phases	3
Number of parallel paths	1
Outer diameter of the stator core [mm]	235
Core length [mm]	195
Air-gap diameter [mm]	145
Radial air-gap length [mm]	0.45
Number of stator slots	36
Number of rotor slots	34
Skew of rotor slots	0
Mass of the rotor [kg]	30
Connection	Delta
Rated voltage [V]	380
Rated frequency [Hz]	50
Rated current [A]	28
Rated power [kW]	15

Using the magnetic bearings, the rotor was forced to move along a trajectory

$$p_{C1}(t) = p_{C10} + p_{1\Omega}e^{i\Omega t} + p_{\omega}e^{i\omega t},$$
$$p_{C2}(t) = p_{C20} + p_{2\Omega}e^{i\Omega t} + p_{\omega}e^{i\omega t}, \qquad (8)$$

where Ω is rotation frequency, ω is whirling frequency, p_ω is whirling radius (defined as real and positive) and subscripts 1 and 2 refer to the two rotor ends.

The control system, which was used to achieve this orbit, is shown in Figure 1. It is a fairly standard unbalance compensation scheme, except that reference orbits are not zero and there are two frequencies to deal with. Suitable coefficients $a(\Omega)$ and $a(\omega)$ were determined using methods presented by Lantto [7]. The control system was realised with a prototype digital controller built in the Laboratory of Electromechanics.

Because of the mechanical tolerances, the electrical motor was not perfectly aligned with the magnetic bearing position sensors neither in the rotor or stator. This misalignment can be compensated by the first two terms in Eq. (8). We must determine the parameters p_{C10}, p_{C20}, $p_{1\Omega}$ and $p_{2\Omega}$ so that they define a rotor trajectory, in which the rotor core is concentric with the stator core. This trajectory was obtained from a calibration procedure [8], which is sketched in the following: The rotor was locked to some rotation angle. A DC-current was fed into the stator winding and the magnetic bearings were used to measure the static force caused by this current. By using the magnetic bearings as force sensors and switching the DC-current on and off, such a position combination (p_{C1},p_{C2}) was searched for in which the electrical motor did not cause any forces. This procedure was repeated for numerous rotation angles. The calibration procedure defines the trajectory along which the rotor should move in the position sensors to produces a zero force. Fortunately, and according to the theory, these orbits are circular and they can be realised according to Eq. (8). Thus when the trajectory of Eq. (8) is used, the rotor follows a cylindrical orbit around the centreline of the stator. The frequency of this movement is ω and radius is p_ω.

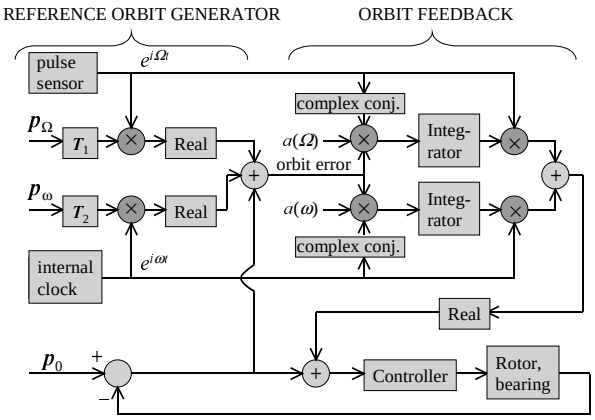

FIGURE 1: Control system.

The bearing forces were measured using the magnetic bearings as force sensors. Let us denote the control currents in X and Y directions $I_{Xn}(t)$ and $I_{Yn}(t)$ where n=1 or 2 refers to the two ends of the machine. The whirling frequency current components were computed as

$$I_{(X/Y)n\omega} = \frac{2}{T}\int_T I_{(X/Y)n}(t)e^{-i\omega t}dt, \qquad (9)$$

where T is a time long enough to give reliable results. The relationship between the control current and bearing force was measured and found to be linear in the normal operation range of the bearings. Using the measured current stiffness coefficients $h_{f(X,Y)n}$, the whirling frequency components of the bearing forces are obtained as

$$F_{X1\omega} = h_{fX1} I_{Y1\omega}\,,\; F_{Y1\omega} = h_{fY1} I_{Y1\omega}\,,$$
$$F_{X2\omega} = h_{fX2} I_{X2\omega}\,,\; F_{Y2\omega} = h_{fY2} I_{Y2\omega}\,. \qquad (10)$$

For each supply voltage – whirling frequency combination, the force was measured twice. In both the cases, the rotor was in whirling motion. In the first measurement, the motor running at no load was fed by the specified voltage U. In the second measurement, the supply voltage was zero and the rotor not rotating. From these measurements, the bearing force differences were computed

$$\Delta F_{X1\omega} = F_{X1\omega}(U) - F_{X1\omega}(0)\,. \qquad (11)$$

The total force, caused by the electrical motor, is supposed to be

$$F_{Cmtot}(t) = F_{mX}(t) + iF_{mY}(t) = F_{m\omega+}e^{i\omega t} + F_{m\omega-}e^{-i\omega t}\,, \qquad (12)$$

where $F_{m\omega+}$ is a force rotating in the same direction as the whirling motion and $F_{m\omega-}$ is the force component rotating in the opposite direction.
The whirling frequency rotor forces were computed from the bearing forces as

$$F_{m\omega+} = \left(\Delta F_{X1\omega} + \Delta F_{X2\omega} + i\Delta F_{Y1\omega} + i\Delta F_{Y2\omega}\right)/2,$$
$$F_{m\omega-} = \left(\Delta F^{*}_{X1\omega} + \Delta F^{*}_{X2\omega} + i\Delta F^{*}_{Y1\omega} + i\Delta F^{*}_{Y2\omega}\right)/2, \qquad (13)$$

where superscript * denotes a complex conjugate. In the circular whirling motion considered, the backward rotating force component $F_{m\omega-}$ should be zero. In the tests, it was computed and verified to be negligible compared with the forward rotating force.
The shaft of the standard motor is flexible. The large magnetic forces caused some bending that disturbed the measurements. The effect of bending was eliminated from the results measured at the synchronous whirling speed by using a rotor dynamic model. The parameters of the rotor model were adjusted by fitting the two first natural frequencies to the measured values.

4 RESULTS

4.1 Verification of the finite element analysis

Figure 2 shows the radial and tangential components of the force computed and measured for the test motor as functions of the whirling frequency. The whirling radius is 50 μm, and the unloaded motor is supplied from a 230 V sinusoidal, three-phase voltage source. The supply voltage was reduced from the rated 380 V to keep the magnetic bearings at their linear range of operation and guarantee an accurate force measurement for the whole range of the whirling frequency.

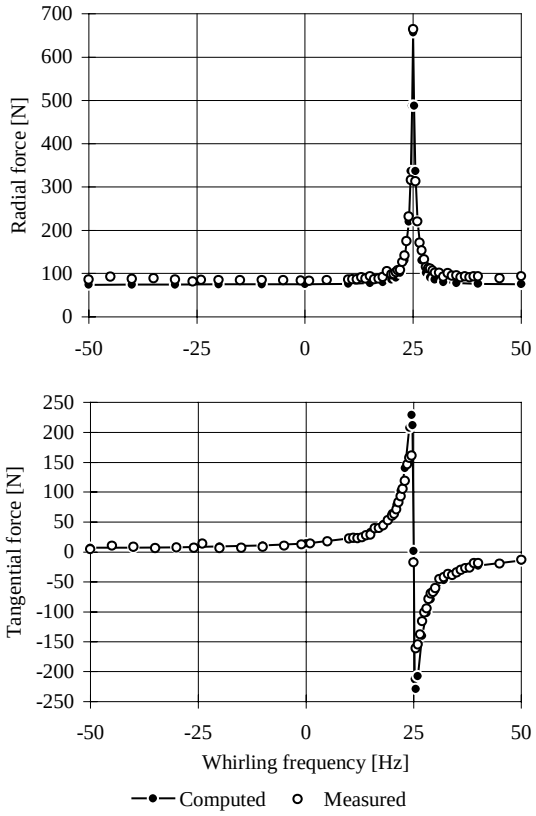

FIGURE 2: Radial and tangential forces measured and computed for the motor at no load.

The radial force has a sharp maximum at 25 Hz whirling frequency. As discussed in Section 2.2, the eccentricity produces two additional flux-density waves with pole numbers $p\pm1$ into the air gap. These eccentricity harmonics usually move at a speed different from the speed of the rotor. Thus, the flux density is time-dependent and induces currents in the rotor cage. The currents oppose the change of the flux, equalise the flux distribution and reduce the radial force. At the 25 Hz whirling frequency, both the eccentricity harmonics have zero slip with respect to the rotor i.e. they are static fields. No equalising currents are induced, and the maximum in the radial force occurs.
The agreement between the measured and computed forces is good. The largest difference occurs in the tangential force around the 25 Hz whirling frequency. It may be that we were not able to maintain a constant whirling speed when measuring close to the tangential force maximums but the speed fluctuated. The forces measured as time-averages are thus smaller than the maximum value.
Figure 3 shows the calculated and measured radial force as functions of the whirling radius. The whirling frequency is 25 Hz, and the supply voltage has been used as a parameter. The force increases linearly with the relative eccentricity.

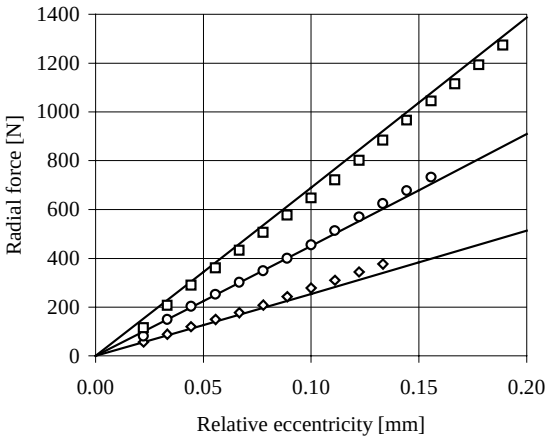

FIGURE 3: Radial force measured and computed for the unloaded motor as function of eccentricity at 25 Hz whirling frequency. The curves from the bottom to the top are associated with the supply voltages 150, 200 and 250 V. The solid lines show the computed forces.

As already discussed, it is difficult to take the magnetic saturation of iron into account within analytic models. The results of the analytic model [1] are compared with the results of the FEM computation in Figure 4, which shows the radial force as function of the supply voltage in the case of dynamic eccentricity i.e. at 25 Hz whirling frequency. At small voltages, the iron core is non-saturated, and the forces predicted by the two methods agree. At higher voltages, the saturation of iron suppresses the eccentricity harmonics and reduces the force. The analytic method does not model this effect.
The different operation states of the machine and the effects of machine constructions on the forces are studied in more detail in reference [9].

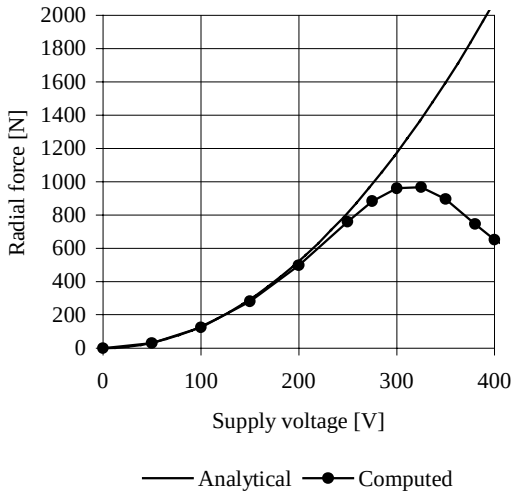

FIGURE 4: Radial force calculated for the motor as function of the supply voltage at no load and 25 Hz whirling frequency. The analytic model neglects the magnetic saturation of iron. The rated voltage of the motor is 380 V.

4.2 Validation of the low-order model

In spite of the strong magnetic non-linearity, the spatial dependence of the measured and computed forces proved to be linear. This justifies the use of Eqs. (6) and (7) for the saturated operation points. The parameters fitted for the low-order model are given in Table 2.

TABLE 2: Parameters of the low-order model for the 15 kW test motor supplied by the rated voltage.

Parameter	No load	Half load	Rated load
k_0 [MN/m]	4.13	4.89	6.22
k_{p-1} [MN/ms]	8.37	9.10	15.7
k_{p+1} [MN/ms]	94.7	102.5	74.9
z_{p-1} [1/s]	–0.59x2π +25.0x2π *i*	–0.42x2π +25.4x2π *i*	–0.50x2π +25.8x2π *i*
z_{p+1} [1/s]	–1.70x2π +25.0x2π *i*	–2.09x2π +23.8x2π i	–1.68x2π +22.6x2π *i*

In Figure 5, the frequency response functions obtained from the low-order model are compared with the ones from FE-analysis in the case of a loaded motor. The loading affects the radial and tangential forces. The single maximum in the radial force of the unloaded motor is divided into two. The eccentricity harmonics p–1 and p+1 have their zero slips at whirling frequencies 25.80 and 22.60 Hz (Eq. 3, s=0.032). At these frequencies, the corresponding harmonic rotor currents are zero, and as the flux-density harmonics are not damped, they have maximum amplitudes. The radial force has two local maximums close to those whirling frequencies at which the harmonics have zero slips.

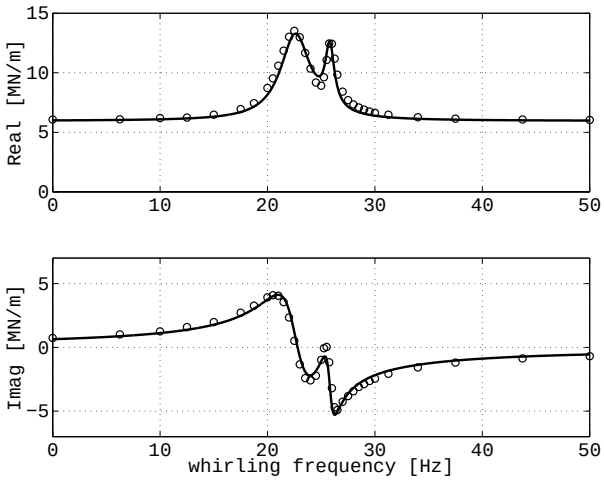

FIGURE 5: Frequency response function computed for the motor at rated load. The thick line presents Eq. (6); the circles denote the results from FE-analysis.

Let us study next, how well Eq. (7) predicts a transient response. For this purpose, the rotor is displaced from the central position for a short period of time and the response to this displacement is studied using both Eq.

(7) and FE analysis. The results are shown in Figure 6. Eq. (7) predicts the low frequency component of the transient force as well as the finite element analysis. There is a relatively large high-frequency component associated with the slotting, which is not predicted.

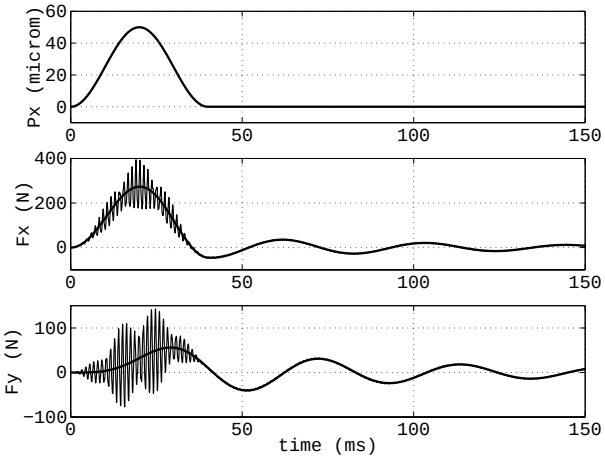

FIGURE 6: Comparison of the transient responses obtained using the low-order model and FE-analysis. The thicker line is associated with the low-order model.

4.3 Some rotor dynamic implications

The radial force decreases the mechanical resonance frequencies and critical speeds. It increases the unbalance response at speeds below the first critical speed i.e. it increases the vibration amplitudes and synchronous bearing forces. Note that the unbalance excitation frequency is exactly the mechanical rotation frequency, and therefore, it occurs near the force peaks shown in Figures 2 and 5.

The tangential force component has a destabilising effect on those forward rotating whirling modes for which the natural frequency is below the rotating speed. This effect is strongest when the rotational speed is slightly higher than the natural frequency.

The high frequency force component, shown in Figure 6, may generate considerable acoustic noise when the frequency of the force matches with a mechanical resonance frequency of the structure. An important feature of the high frequency force component is that the amplitude is dependent on rotor position.

Because the air gap of a standard induction motor is small, the negative spring effect may become large compared to magnetic bearing stiffness. The situation is especially difficult when the rotation speed, and the resonance peaks seen in Figures 2 and 5, is below the gain crossover frequency of the position control loop. This was the case in our test machine. Even though the bearings worked well when at small supply voltages, we had to increase the bearing stiffness considerably to be able to measure at higher supply voltages. In case of frequency converter fed high speed machines, a good method to overcome this difficulty is to use a quadratic voltage ramp when running the machine up.

CONCLUSIONS

The electromagnetic force acting on a whirling cage rotor has been studied. The magnetic field of the cage induction motor was solved using time-stepping finite element analysis, and the force was computed from the air-gap magnetic field. A standard 15 kW four-pole induction motor was equipped with active magnetic bearings to obtain a test machine for verifying the method of force calculation. The whirling motion was achieved by a proper control of the magnetic bearings. The bearings were also calibrated to measure the force acting between the rotor and stator. The measured and computed forces show good agreement. The numerically computed forces were fitted to a simple second order transfer function model. The fit seems to be excellent. This implies that a relatively simple force model can be used as first approximation when studying the effects of the magnetic forces on rotor dynamics.

REFERENCES

1. Früchtenicht J. et al., Exzentrizitätsfelder als Ursache von Laufinstabillitäten bei Asynchronmachinen. Parts 1 and 2. Archiv für Electrotechnik 65 (1982), pp. 271–292.
2. Arkkio A. and Lindgren O., Finite element analysis of the magnetic forces acting on an eccentric rotor of a high-speed induction motor. Proceedings of the 4th International Symposium on Magnetic Bearings. 23–26 August 1994, Zurich, Switzerland, pp. 225–230.
3. Arkkio A., Analysis of induction motors based on the numerical solution of the magnetic field and circuit equations. Helsinki 1987, Acta Polytechnica Scandinavica, El. Eng. Series, No. 59. 97 p.
4. Coulomb J.L., A Methodology for the determination of global electromechanical quantities from a finite element analysis and its application to the evaluation of magnetic forces, torques and stiffness. IEEE Trans. on Magnetics, 19 (1983) 6, pp. 2514–2519.
5. Sadowski N. et al., Finite element torque calculation in electrical machines while considering the movement. IEEE Trans. on Magnetics, 28 (1992) 2, pp. 1410–1413.
6. Antila M. et al., Determination of Forces and linearized parameters of radial active magnetic bearings by finite element technique. IEEE Trans. on Magnetics, 34 (1998) 3, pp. 684–694.
7. Lantto E., Robust control of magnetic bearings in subcritical machines. Helsinki 1999, Acta Polytechnica Scandinavica, El. Eng. Series, No. 94. 143 p.
8. Simon A., Use of magnetic bearings to measure the forces caused by an eccentric rotor in an induction motor. Master of Science thesis. Technical Univ. of Budapest, Faculty of Electrical Engineering and Informatics, 1999, 80 p.
9. Arkkio A. et al., Electromagnetic force on a whirling cage rotor, Paper accepted for publication in IEE Proceedings – Electric Power Applications.